藏南彭措林埃达克质岩脉的岩石成因及对区域成矿作用的启示*

裴英茹[1,2,3] 杨竹森[3**] 郑远川[2] 侯增谦[4] 田世洪[3] 刘英超[4] 赵晓燕[3] 周金胜[4]

PEI YingRu[1,2,3], YANG ZhuSen[3**], ZHENG YuanChuan[2], HOU ZengQian[4], TIAN ShiHong[3], LIU YingChao[4], ZHAO XiaoYan[3] and ZHOU JinSheng[4]

1. 中国地质科学院地质力学研究所,北京 100081
2. 中国地质大学地球科学与资源学院,北京 100083
3. 中国地质科学院矿产资源研究所,北京 100037
4. 中国地质科学院地质研究所,北京 100037

1. *Institute of Geomechanics, Chinese Academy of Geological Sciences, Beijing* 100081, *China*
2. *School of Earth Sciences and Resources, China University of Geosciences, Beijing* 100083, *China*
3. *Institute of Mineral Resources, Chinese Academy of Geological Sciences, Beijing* 100037, *China*
4. *Institute of Geology, Chinese Academy of Geological Sciences, Beijing* 100037, *China*

2015-06-26 收稿; 2015-12-03 改回.

Pei YR, Yang ZS, Zheng YC, Hou ZQ, Tian SH, Liu YC, Zhao XY and Zhou JS. 2017. The geochemical characteristics of the Pengcuolin adakitic dykes, southern Tibet: Petrogenesis and implications for regional metallogenesis. *Acta Petrologica Sinica*, 33(2):515 – 528

Abstract The Pengcuolin dykes are located in the west part of the central Gangdese porphyry copper belt, southern Tibet, and they intruded into the Gangdese batholith with width of 3 ~ 5m. LA-ICP-MS U-Pb dating of zircons from two dyke samples yield ages of 9.7 ±0.2Ma and 9.9 ±0.3Ma. Geochemical analyses indicate that they are characterized by high SiO_2 contents (67.05% ~69.96%), K_2O ranging from 6.05% to 6.88%, MgO from 0.47% to 1.27%, enriched in light rare earth elements (LREE) and large ion lithophile elements (LILE) but depleted in high field strength elements (HFSE), relatively high Sr/Y (45.5 ~ 80.0) and La/Yb (75.7 ~ 110) ratios, showing adakitic affinities. Compared with the Miocene porphyries in the Gangdese porphyry copper belt, the dykes have higher initial $^{87}Sr/^{86}Sr_{(i)}$ (0.7120 ~ 0.7123), $^{206}Pb/^{204}Pb$ (18.812 ~ 18.844), $^{207}Pb/^{204}Pb$ (15.705 ~ 15.728), $^{208}Pb/^{204}Pb$ (39.424 ~ 39.523) ratios, but lower $\varepsilon_{Nd}(t)$ values (−10.9 ~ −9.8) and older Nd model ages (t_{DM} = 1.36 ~ 1.43Ga). The above geochemical data indicates that the dykes were probably derived from an overthickened lower crust with minor mantle material, and more old crust material have been involved than the Miocene porphyries in the same belt. Meanwhile, the zircon trace element analysis show that they possess low fO_2 values (ΔFMQ = −6.7 ~ +2.1, average = −1.4). Thus the absence of regional metallogenesis is likely attributed to: (1) the limited sulfide cumulated in the lower crust as a result of the underplating of former arc basalitic magmas; (2) the low fO_2 that are not favor to ore-forming metal. Combining with previous study, it suggests that contribution of juvenile mantle components to the lower crust beneath the south Tibet is the key factor for mineralization in the Gangdese porphyry Cu belt.

Key words Adakitic dykes; Miocene; Petrogenesis; Metallogenesis; Pengcuolin, southern Tibet

摘 要 彭措林岩脉群位于藏南冈底斯斑岩铜矿带中段的西侧,宽约 3 ~ 5m,呈近南北向穿截冈底斯岩基。两组样品的锆石 U-Pb 定年结果为 9.7 ±0.2Ma 和 9.9 ±0.3Ma。岩石地球化学研究显示,岩石以高 SiO_2(67.05% ~69.96%)、K_2O(6.05% ~6.88%)和低 MgO(0.47% ~1.27%)为特征,高度富集轻稀土元素(LREE)和大离子亲石元素(LILE),亏损高场强元素(HFSE),具有高 Sr/Y 和 La/Yb 比值,表现出埃达克岩地球化学亲合性。相对冈底斯中新世埃达克质斑岩而言,该岩脉更加

* 本文受国家重点研发计划(2016YFC0600306)、国家重点基础研究发展计划("973"计划)(2011CB403104)、中国地质调查局项目(12120113037901)和国家科技支撑计划(2006BAB01A04)联合资助.

第一作者简介: 裴英茹,女,1988 年生,博士,矿物学、岩石学、矿床学专业,E-mail: peiyingru@126.com

** **通讯作者**:杨竹森,男,1964 年生,博士,研究员,从事矿床学和矿床地球化学研究,E-mail: yangzhusen@vip.sina.com

富集放射性成因 Sr、Pb 同位素($^{87}Sr/^{86}Sr_{(i)}$ = 0.7120 ~ 0.7123, $^{206}Pb/^{204}Pb$ = 18.812 ~ 18.844, $^{207}Pb/^{204}Pb$ = 15.705 ~ 15.728, $^{208}Pb/^{204}Pb$ = 39.424 ~ 39.523)、具更低的 Nd 同位素值($\varepsilon_{Nd}(t)$ = -10.9 ~ -9.8)和更为古老的 Nd 模式年龄(t_{DM} = 1.36 ~ 1.43Ga)。以上地球化学分析表明,彭措林岩脉很可能起源于加厚的古老下地壳,相较于冈底斯斑岩铜矿带内其他的中新世斑岩而言,其岩浆源区含有更少的幔源组分和更多的古老地壳组分。锆石微量元素结果显示,岩脉的氧逸度较低(ΔFMQ = -6.7 ~ +2.1,平均值为 -1.4)。故而,彭措林埃达克质岩脉不具备区域成矿潜力的原因可以归结如下:(1)下地壳岩浆源区中新生幔源组分含量较少,指示了古老下地壳中岛弧幔源岩浆注入量较少,因而岛弧期堆晶至下地壳的金属硫化物极为有限;(2)较低的氧逸度导致岩浆萃取金属的能力相对较弱。结合前人研究可知,下地壳中新生幔源组分的贡献率是影响冈底斯斑岩铜矿带后碰撞埃达克岩能否成矿的关键因素。

关键词 埃达克质岩脉;中新世;岩石成因;成矿作用;藏南彭措林

中图法分类号 P581.13;P597.3

1 引言

近年来的研究表明斑岩型矿床除了可以产出于岛弧及陆缘弧环境外(Sillitoe, 1972, 2010),也可产出于陆内碰撞造山带,并以青藏高原后碰撞伸展环境产出的冈底斯斑岩铜矿带最为典型(侯增谦等, 2001; 郑有业等, 2004a, b; Qu *et al.*, 2007; Hou *et al.*, 2004; Hou and Cook, 2009; Zheng *et al.*, 2012a; 秦克章等, 2014; Yang *et al.*, 2016)。冈底斯斑岩铜矿带位于雅鲁藏布江缝合带北侧、拉萨地体南缘的冈底斯构造-岩浆带中,被分为东、中、西三段(侯增谦等, 2006a, b; Zheng *et al.*, 2012b; Hou *et al.*, 2013)。在冈底斯斑岩铜矿带中段(87°30′E ~ 92°10′E, Hou *et al.*, 2013),典型斑岩铜矿床驱龙、厅宫、冲江、甲马、南木等的埃达克质含矿斑岩年龄为 17 ~ 14Ma(侯增谦, 2003; Chung *et al.*, 2003; 郑有业等, 2004a, b; 芮宗瑶等, 2004; Hou *et al.*, 2004; Hou and Cook, 2009; Qu *et al.*, 2007; Xu *et al.*, 2010; Li *et al.*, 2011; Yang *et al.*, 2016);而与成矿密切相关的埃达克质岩浆作用从 30Ma 持续到 13Ma,并在 16Ma 达到高峰期(Chung *et al.*, 2003; Hou *et al.*, 2004, 2013; Qu *et al.*, 2007; Zheng *et al.*, 2012a)。相对的,冈底斯中新世不含矿斑岩的年龄为 25 ~ 14Ma(Hou *et al.*, 2015a)。作为冈底斯斑岩铜矿带中段最西缘的斑岩型铜矿床,朱诺(29°39′N,87°28′E)含矿斑岩成岩年龄为 15.6Ma、成矿年龄为 13.7Ma,它的发现将传统意义上的冈底斯斑岩铜矿带向西延伸了 100km(郑有业等, 2007; 黄勇等, 2015)。相较于冈底斯斑岩铜矿带中新世埃达克质含矿斑岩起源于加厚的新生铁镁质下地壳(Hou *et al.*, 2013; Yang *et al.*, 2016),朱诺花岗岩富集 Hf 同位素($\varepsilon_{Hf}(t)$ = -9.87 ~ 0.21),并具有古老二阶段模式年龄(1.08 ~ 1.73Ga),可能指示古老拉萨地体的印迹(黄勇等, 2015)。通过对比冈底斯斑岩铜矿带中新世含矿斑岩与不含矿斑岩,发现幔源组分的贡献对中新世埃达克质斑岩是否成矿起着至关重要的作用(Hou *et al.*, 2013)。

在冈底斯斑岩铜矿带中段,关于 14Ma 之后是否还存在埃达克质斑岩的问题尚未报道。同时,除了朱诺矿床,南拉萨地体 87°E 以东的新生下地壳(Hou *et al.*, 2015b)是否还存在局部地壳基底组成的不均一性等问题值得开展更多的研究。本文对彭措林(29°24′N、88°00′E)埃达克质岩脉进行了细致的锆石 LA-ICP-MS U-Pb 年龄、岩石地球化学和 Sr-Nd-Pb 同位素特征研究,通过与冈底斯斑岩铜矿带中段埃达克质含矿斑岩、不含矿斑岩的对比,探讨了彭措林岩脉的岩石成因和对区域成矿作用的启示,并初步揭示冈底斯斑岩铜矿带中段地壳基底组成的不均一性。

2 地质背景与样品特征

因印-亚陆陆碰撞产生的喜马拉雅-西藏造山带从北向南依次由松潘-甘孜地体、羌塘地体和拉萨地体组成,其构造界线分别为金沙江缝合带、班公湖怒江缝合带和雅鲁藏布江缝合带(Yin and Harrison, 2000)。其中,拉萨地体以雅鲁藏布江缝合带(IYZSZ)和班公湖怒江缝合带(BNSZ)为南、北构造界线,被狮泉河-纳木错蛇绿岩带(SNMZ)和洛巴堆-米拉山断裂(LMF)分为北拉萨地体、中拉萨地体和南拉萨地体等三个构造单元(图 1a, Zhu *et al.*, 2011)。冈底斯斑岩铜矿带主要分布在南拉萨地体的南缘、雅鲁藏布江缝合带北侧(侯增谦等, 2006a),其含矿斑岩体侵位受近 EW 向展布的冈底斯弧花岗岩基和近 NS 向正断层系统控制(侯增谦等, 2004);成矿岩体以高钾钙碱性为主,岩石组合以花岗闪长岩-二长花岗岩-花岗斑岩为主,富集大离子亲石元素(LILE),亏损高场强元素(HFSE),成岩成矿时代主要集中在中新世(侯增谦等, 2012)。在成矿最有利的冈底斯斑岩铜矿带中段(87°30′E ~ 92°10′E, Hou *et al.*, 2013)存在驱龙、厅宫、冲江、甲马、南木等典型斑岩铜矿床。其中,朱诺斑岩型矿床位于冈底斯斑岩铜矿带中段最西缘,为冈底斯斑岩铜矿带中段含矿斑岩年龄、岩浆源区及成矿作用等问题的研究提供了更多认识(郑有业等, 2007; 黄勇等, 2015)。

研究区位于南拉萨地体中段拉孜县彭措林村(29°24′N、88°00′E),地处冈底斯斑岩铜矿带中段的西缘,在朱诺矿床东南方向约 59km 处。区内发育的一系列宽约 3 ~ 5m 的 NS 向及 NNW 向岩脉群,穿切白垩纪花岗闪长岩和石英正长岩,位于近南北向断裂之中(图 1a),可能与青藏高原在后碰撞晚期阶段因 EW 向地壳伸展(<18Ma)形成的 NS 向正断层

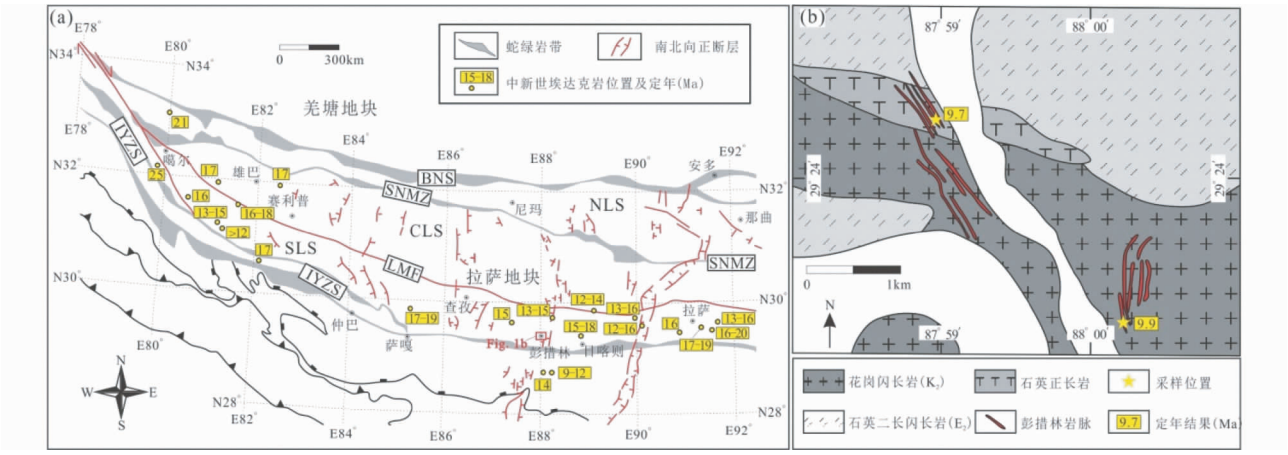

图 1 藏南中新世埃达克岩时空分布图(a,据 Zhu *et al.*, 2011; Zheng *et al.*, 2012b; Liu *et al.*, 2014 修改)和彭措林地质简图(b,据湖北省地质调查院,2003①改绘)

IYZS-印度-雅鲁藏布缝合带;BNS-班公湖-怒江缝合带;SNMZ-狮泉河-纳木错蛇绿混杂岩带;LMF-洛巴堆-米拉山断裂;NLS-北拉萨地体;CLS-中拉萨地体;SLS-南拉萨地体

Fig. 1 Simplified geological map for the spatial distribution of the Miocene adakitic rocks in southern Tibet (a, modified after Zhu *et al.*, 2011; Zheng *et al.*, 2012b; Liu *et al.*, 2014) and simplified geological map of Pengcuolin (b)

IYZS-Indus-Yarlung Zangbo Suture Zone; BNS-Bangong Co-Nujiang Suture Zone; SNMZ-Shiquan River-Nam Tso Ophiolitic Melange Zone; LMF-Luobadui-Milashan Fault; NLS-Nothern Lhasa subterrane; CLS-Central Lhasa subterrane; SLS-Southern Lhasa subterrane

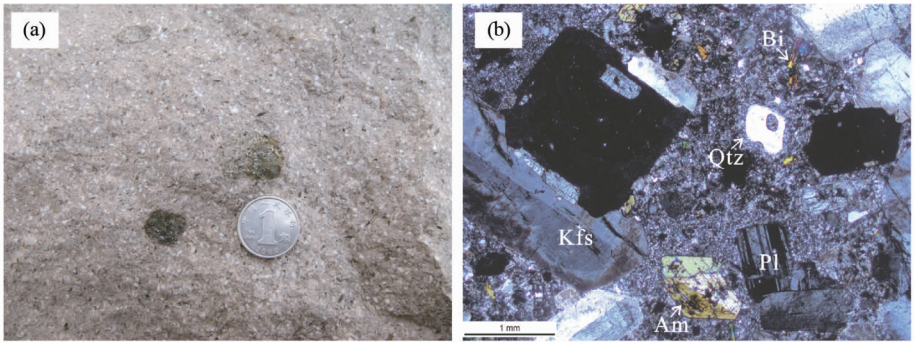

图 2 藏南彭措林岩脉野外照片(a)和显微照片(b)

Kfs-钾长石;Pl-斜长石;Qtz-石英;Am-角闪石;Bi-黑云母

Fig. 2 Field photograph (a) and microphotograph (b) for dykes in Pengcuolin, southern Tibet

Kfs-potash feldspar; Pl-plagioclase; Qtz-quartz; Am-amphibole; Bi-biotite

系统(14~10Ma)有关(侯增谦等, 2006a)。本文所采岩脉中岩石呈浅肉红色,具斑状结构(图 2a)。斑晶含量约 30%,主要为钾长石、斜长石和石英,以及少量角闪石和黑云母。钾长石斑晶呈半自形-自形板状,具卡式双晶,部分颗粒表面泥化比较明显,偶见环带状构造;斜长石斑晶多呈自形板状,具聚片双晶;石英斑晶多呈他形粒状,部分被熔蚀成港湾状;角闪石斑晶呈长条状或菱形,单偏光下为黄绿色;黑云母斑晶呈长条状或宽片状,单偏光下为棕褐色;基质主要由石英、斜长石和黑云母等矿物组成(图 2b)。

3 分析方法

3.1 锆石 U-Pb 定年及微量元素

将挑选出的锆石制成环氧树脂样品靶,经过打磨抛光使锆石露出中心后进行反射光、透射光和阴极发光(CL)显微照相。锆石 U-Pb 同位素定年和微量元素在西北大学大陆动力学国家重点实验室利用 LA-ICP-MS 分析完成(袁洪林, 2012)。激光剥蚀系统为 GeoLas 2005,电感耦合等离子质谱

① 湖北省地质调查院. 2003. 1∶250000 拉孜县幅区域地质调查报告

表 1 藏南彭措林岩脉锆石 U-Pb 年龄数据

Table 1 U-Pb age data of zircons from dykes in Pengcuolin, southern Tibet

测点号	Th($\times10^{-6}$)	U($\times10^{-6}$)	Th/U	$^{207}Pb/^{206}Pb$	$\pm1\sigma$	$^{207}Pb/^{235}U$	$\pm1\sigma$	$^{206}Pb/^{238}Pb$	$\pm1\sigma$	$^{206}Pb/^{238}Pb$(Ma)	$\pm1\sigma$
PCL09-1-2-01	9258	3951	2.34	0.0507	0.0027	0.0104	0.0005	0.0015	0.00003	9.6	0.2
PCL09-1-2-02	2637	2786	0.95	0.0487	0.0029	0.0099	0.0005	0.0015	0.00003	9.5	0.2
PCL09-1-2-03	473.1	357.4	1.32	0.0483	0.0156	0.0094	0.0030	0.0014	0.00007	9.1	0.5
PCL09-1-2-04	1190	1640	0.73	0.0488	0.0039	0.0102	0.0008	0.0015	0.00003	9.7	0.2
PCL09-1-2-05	3133	1618	1.94	0.0512	0.0071	0.0108	0.0015	0.0015	0.00005	9.8	0.3
PCL09-1-2-06	3886	1147	3.39	0.0520	0.0041	0.0106	0.0008	0.0015	0.00003	9.5	0.2
PCL09-1-2-07	11003	2144	5.13	0.0490	0.0032	0.0101	0.0006	0.0015	0.00003	9.6	0.2
PCL09-1-2-08	5186	1878	2.76	0.0493	0.0053	0.0108	0.0011	0.0016	0.00004	10.2	0.3
PCL09-1-2-09	5336	3017	1.77	0.0481	0.0026	0.0100	0.0005	0.0015	0.00003	9.7	0.2
PCL09-1-2-11	2456	1331	1.85	0.0574	0.0060	0.0112	0.0011	0.0014	0.00004	9.1	0.3
PCL09-1-2-12	5306	1723	3.08	0.0535	0.0053	0.0106	0.0010	0.0014	0.00004	9.2	0.2
PCL09-1-2-13	102.7	246.9	0.42	0.0559	0.0141	0.0127	0.0031	0.0017	0.00008	10.6	0.5
PCL09-1-2-14	3261	2151	1.52	0.0444	0.0037	0.0092	0.0007	0.0015	0.00003	9.6	0.2
PCL09-1-2-15	1320	1553	0.85	0.0503	0.0048	0.0103	0.0009	0.0015	0.00004	9.6	0.2
PCL09-1-2-16	1078	1257	0.86	0.0467	0.0062	0.0092	0.0012	0.0014	0.00004	9.2	0.3
PCL09-1-2-17	17914	3383	5.30	0.0486	0.0036	0.0106	0.0007	0.0016	0.00003	10.2	0.2
PCL09-1-2-18	446.3	4157	0.11	0.0526	0.0025	0.0114	0.0005	0.0016	0.00003	10.1	0.2
PCL09-2-9-01	1019	1302	0.78	0.0474	0.0039	0.0096	0.0008	0.0015	0.00003	9.5	0.2
PCL09-2-9-02	5784	1899	3.05	0.0488	0.0076	0.0102	0.0015	0.0015	0.00004	9.8	0.3
PCL09-2-9-03	666.4	1054	0.63	0.0479	0.0056	0.0104	0.0012	0.0016	0.00004	10.2	0.3
PCL09-2-9-04	4099	1896	2.16	0.0489	0.0069	0.0105	0.0015	0.0016	0.00004	10.0	0.2
PCL09-2-9-06	7745	3646	2.12	0.0586	0.0050	0.0125	0.0010	0.0016	0.00004	10.0	0.2
PCL09-2-9-07	1174	585	2.01	0.0452	0.0118	0.0096	0.0025	0.0015	0.00008	9.9	0.5
PCL09-2-9-09	2513	1439	1.75	0.0481	0.0075	0.0106	0.0016	0.0016	0.00005	10.3	0.4
PCL09-2-9-10	1461	1335	1.09	0.0480	0.0055	0.0102	0.0011	0.0016	0.00004	10.0	0.3
PCL09-2-9-11	545.6	934.7	0.58	0.0596	0.0091	0.0134	0.0020	0.0016	0.00006	10.5	0.4
PCL09-2-9-13	52907	13441	3.94	0.0535	0.0128	0.0101	0.0024	0.0014	0.00008	8.8	0.5
PCL09-2-9-14	2884	2620	1.10	0.0626	0.0055	0.0138	0.0011	0.0016	0.00004	10.3	0.3
PCL09-2-9-15	6741	3133	2.15	0.0559	0.0086	0.0122	0.0018	0.0016	0.00005	10.2	0.3
PCL09-2-9-18	1202	719.0	1.67	0.0734	0.0082	0.0137	0.0015	0.0014	0.00004	8.7	0.3

(ICP-MS)为 Agilent 7500a。实验过程采用 NIST610、SK10 和 91500 作为标样。采用 Andersen (2002)进行普通铅校正。锆石 U-Pb 年龄谐和图的绘制和 MSWD 的计算均采用 Isoplot/Ex_ver3(Ludwig, 2003)。对于小于 1000Ma 的岩浆锆石采用$^{206}Pb/^{238}U$ 年龄,对于大于 1000Ma 的岩浆锆石采用$^{207}Pb/^{206}Pb$ 年龄,测试结果见表 1。

通过锆石微量元素计算 Ce 异常(Blundy and Wood, 1994; Qiu *et al.*, 2013)和 Ti 温度计(Watson and Harrison, 2005),从而得到氧逸度(Trail *et al.*, 2011, 2012)。Ce 异常根据晶格应变模型由 Nd、Sm 和 Gd 至 Lu 的锆石微量元素计算(Blundy and Wood, 1994; Qiu *et al.*, 2013)。具体采用公式如下:

$$Lg(Ti) = 6.01 \pm 0.3 - (5080 \pm 30)/T$$

$$\ln(Ce/Ce^{*})_D = (0.1156 \pm 0.0050) \times \ln(fO_2) + (13860 \pm 708)/T - 6.125 \pm 0.484$$

其中,fO_2 为氧逸度,T 为绝对温度(K)。锆石微量数据见表 2。

3.2 全岩主、微量元素

全岩主、微量元素在核工业北京地质研究院分析测试研究中心进行,测试结果见表 3。全岩主量元素根据 GB/T14506.28-93 硅酸盐岩石化学分析方法、采用飞利浦 PW2404 X 射线荧光光谱仪进行测定,FeO 的含量采用滴定法测定;全岩微量元素根据 DZ/T0223-2001 电感耦合等离子体质谱(ICP-MS)方法、采用 Finnigan MAT 制造的 HR-ICP-MS 进行测定。

3.3 Sr-Nd-Pb 同位素

Sr-Nd-Pb 同位素测试在核工业北京地质研究院分析测试研究中心进行,测试结果见表 4。根据 GB/T17672-1999《岩石中铅锶钕同位素测定方法》,Sr-Nd 同位素由仪器 PHOENIX 测得,Pb 同位素由仪器 ISOPROBE-T 测得。

表 2 藏南彭措林岩脉锆石微量元素数据($\times 10^{-6}$)

Table 2 Trace element data for zircons from dykes in Pengcuolin, southern Tibet ($\times 10^{-6}$)

测点号	La	Ce	Pr	Nd	Sm	Eu	Gd	Tb	Dy	Ho	Er	Tm	Yb	Lu
PCL09-1-2-01	0.20	269.5	1.32	19.4	29.4	14.8	103.4	26.7	225.4	65.4	248.4	45.8	378.5	58.9
PCL09-1-2-02	0.06	350.8	0.77	12.7	21.0	9.70	69.2	17.4	149.5	45.2	174.6	32.6	278.3	48.2
PCL09-1-2-03	0.02	31.0	0.15	2.80	4.20	2.10	14.5	3.90	34.0	10.1	40.3	7.60	67.5	12.5
PCL09-1-2-05	0.50	70.0	0.63	9.50	10.9	5.20	32.0	7.70	62.2	18.6	72.1	14.0	123.8	22.5
PCL09-1-2-06	0.34	169.3	3.36	46.2	50.1	22.4	132.9	30.7	245.3	71.2	270.4	48.6	409.8	67.9
PCL09-1-2-07	0.64	548.2	5.58	74.6	87.2	40.4	231.8	51.8	390.8	102.8	336.8	55.7	408.7	59.9
PCL09-1-2-08	0.60	385.1	4.37	54.9	51.6	21.4	125.2	28.3	225.5	64.8	242.7	44.2	375.5	63.7
PCL09-1-2-09	0.35	350.0	2.96	42.8	48.7	21.4	125.9	28.1	206.6	53.9	185.2	31.1	250.7	40.3
PCL09-1-2-11	0.33	127.4	0.54	8.30	11.7	4.90	38.2	9.00	71.5	20.6	77.7	14.3	124.8	21.9
PCL09-1-2-12	0.19	177.7	1.44	22.6	30.8	14.6	93.1	23.0	187.8	53.6	197.6	34.3	275.4	45.3
PCL09-1-2-13	0.11	27.1	0.03	0.30	0.60	0.30	2.70	1.00	10.3	4.10	19.5	4.70	49.6	9.70
PCL09-1-2-14	0.36	219.2	1.01	14.2	17.1	7.70	57.7	14.6	127.3	39.1	154.3	30.1	266.7	46.0
PCL09-1-2-15	0.09	74.0	0.21	2.70	4.20	1.60	15.3	4.30	40.2	14.3	64.7	14.7	147.9	29.3
PCL09-1-2-16	0.28	111.7	1.57	17.5	16.6	7.50	42.6	10.3	87.3	26.0	101.7	19.6	172.1	28.7
PCL09-1-2-17	30.13	1157	32.30	284.2	202.2	82.3	423.6	88.2	594.8	158.0	503.7	91.5	735.6	115.0
PCL09-1-2-18	0.03	14.2	0.07	1.60	7.40	1.40	48.7	18.3	188.0	60.2	239.5	44.8	381.3	65.5
PCL09-2-9-01	0.02	64.6	0.12	1.80	3.40	1.10	13.2	3.80	39.0	13.2	55.9	13.5	131.6	25.5
PCL09-2-9-02	0.97	196.7	2.14	28.1	21.7	7.90	52.0	12.8	103.2	30.4	108.7	22.3	191.6	31.5
PCL09-2-9-03	0.36	47.2	0.15	1.40	2.70	1.00	9.90	3.10	31.3	11.4	50.3	12.1	121.5	23.7
PCL09-2-9-04	1.91	226.0	2.96	35.1	37.9	15.0	94.1	23.5	181.5	49.8	166.2	31.2	248.5	38.3
PCL09-2-9-06	2.47	98.5	1.31	10.1	8.80	2.80	24.6	6.40	56.3	18.2	71.6	16.0	149.4	27.4
PCL09-2-9-07	0.05	70.3	0.40	6.70	9.20	4.50	29.3	7.50	63.7	19.5	70.7	14.6	122.6	21.0
PCL09-2-9-09	1.01	170.6	2.14	24.9	28.2	11.5	83.4	21.9	187.2	56.9	209.2	42.4	368.6	63.4
PCL09-2-9-10	1.23	62.2	0.43	3.00	2.90	1.20	11.4	3.40	34.2	11.9	52.5	12.2	125.9	25.8
PCL09-2-9-11	0.78	48.9	0.26	2.20	2.10	1.00	7.5	2.40	24.4	9.50	43.5	10.8	109.9	21.2
PCL09-2-9-13	29.92	1420	16.45	153.5	118.2	44.6	280.7	58.4	433.7	115.0	380.6	70.9	593.9	97.0
PCL09-2-9-14	1.59	76.8	1.32	9.10	7.50	2.80	20.0	5.80	55.3	17.9	73.4	16.8	154.1	23.9
PCL09-2-9-15	218.1	879.6	106.7	463.7	105.7	20.7	107.1	21.5	158.5	45.7	165.7	33.2	297.3	52.1
PCL09-2-9-18	0.04	115.7	0.65	10.9	15.9	7.70	49.8	12.3	103.8	31.1	109.7	21.2	180.0	29.5

4 分析结果

4.1 锆石 U-Pb 定年及微量元素

本文用于锆石 U-Pb 定年的 2 个样品为 PCL09-1-2(29°24′21.2″N、87°58′57.4″E)和 PCL09-2-9(29°23′10″N、88°00′10.2″E),具体位置如图 1b 所示。彭措林岩脉中的锆石单矿物绝大多数颗粒晶形完好,多呈短柱状,浅灰色。从 CL 图中可以看出(图 3a, b),锆石粒径变化范围为 80 ~ 300μm,长宽比介于 1∶1 ~ 2∶1 之间,大多数具有窄的同心振荡环带。除了 PCL09-1-2-13 具有相对低的 Th 含量(103 × 10^{-6})、PCL09-2-9-13 具有十分高的 Th 含量(52907 × 10^{-6})以外,大多数锆石颗粒具有较高的 Th(446 × 10^{-6} ~ 17914 × 10^{-6})、U(357 × 10^{-6} ~ 4157 × 10^{-6})含量。锆石 Th/U 比值(0.1 ~ 5.3)变化范围较大,绝大多数大于 1(表 1)。在剔除继承锆石年龄(104 ~ 91.7Ma)及不谐和的年龄之后,样品 PCL09-1-2 的锆石 $^{206}Pb/^{238}U$ 加权平均年龄为 9.7 ± 0.2Ma(2σ, MSWD = 2.1, n = 17, 图 3c),样品 PCL09-2-9 的锆石 $^{206}Pb/^{238}U$ 加权平均年龄为 9.9 ± 0.3Ma(2σ, MSWD = 3.2, n = 13, 图 3d)。由此可知,彭措林岩脉的成岩时代约为 10Ma,为中新世晚期。作为冈底斯斑岩铜矿带中段西缘出露的中新世埃达克质斑岩,彭措林岩脉的成岩年龄表明,在冈底斯斑岩铜矿带中段的后碰撞埃达克质岩浆作用在 10Ma 左右仍在进行。

此外,较高的 Th/U 比值、强烈的 Ce 正异常、弱的 Eu 负异常以及富集 HREE 的稀土配分模式(图 4a),表明这些锆石为典型的岩浆锆石(Hoskin and Schaltegger, 2003)。通过锆石微量 Ce 异常和 Ti 温度计算可知(图 4b, Blundy and Wood, 1994; Watson and Harrison, 2005; Qiu *et al.*, 2013; Trail *et al.*, 2011, 2012),彭措林岩脉的氧逸度范围为 −23.4 ~ −13.6(平均值为 −18.2),大部分数据点落于 FMQ 和 IW 之间,ΔFMQ = −6.7 ~ +2.1(平均值为 −1.4)。

4.2 全岩主量元素

彭措林岩脉以高 SiO_2(67.05% ~ 69.96%)、K_2O(6.05% ~ 6.88%)和低 MgO(0.47% ~ 1.27%)为特征,Al_2O_3 含量为 14.33% ~ 15.24%,$Mg^{\#}$ 为 36 ~ 54,K_2O/Na_2O 比值为 1.27 ~ 1.80, A/CNK 比值为 0.85 ~ 1.00 (表 3)。根

表 3 藏南彭措林岩脉主量(wt%)、微量($\times10^{-6}$)元素数据

Table 3 Whole rock major element (wt%) and trace element ($\times10^{-6}$) data for dykes in Pengcuolin, southern Tibet

样品号	PCL09-1-2	PCL09-1-3	PCL09-1-4	PCL09-1-5	PCL09-1-6	PCL09-1-7	PCL09-1-8	PCL09-1-19	PCL09-1-20	PCL09-1-21	PCL09-1-22
SiO_2	67.05	67.77	68.05	67.95	67.67	67.76	67.95	67.30	68.48	68.84	67.05
TiO_2	0.33	0.32	0.31	0.32	0.34	0.31	0.31	0.30	0.27	0.33	0.31
Al_2O_3	14.65	14.33	14.81	14.78	14.61	14.75	14.72	14.89	14.88	15.07	14.81
$Fe_2O_3^T$	1.99	2.16	2.07	2.13	2.03	1.83	2.03	1.89	1.89	2.02	1.97
FeO	0.85	0.65	0.65	0.80	1.35	0.25	0.95	1.20	0.75	1.20	1.60
MnO	0.037	0.043	0.042	0.047	0.038	0.040	0.039	0.039	0.041	0.040	0.055
MgO	1.08	1.18	1.23	1.27	1.15	0.88	1.02	0.88	0.79	1.00	0.66
CaO	1.93	1.62	1.49	1.30	1.79	1.32	1.60	1.84	1.58	0.70	2.03
Na_2O	3.86	4.01	4.11	4.12	3.91	4.08	4.11	4.04	4.44	4.04	3.83
K_2O	6.71	6.71	6.46	6.70	6.49	6.49	6.55	6.60	6.56	6.58	6.88
P_2O_5	0.26	0.26	0.24	0.28	0.25	0.23	0.25	0.21	0.22	0.26	0.23
LOI	2.08	1.55	1.14	1.04	1.64	2.26	1.37	1.93	0.82	1.11	2.08
Total	99.88	99.88	99.88	99.85	99.77	99.92	99.84	99.79	99.89	99.86	99.73
K_2O/Na_2O	1.74	1.67	1.57	1.63	1.66	1.59	1.59	1.63	1.48	1.63	1.80
$Mg^{\#}$	51.8	52.0	54.1	54.2	52.9	48.8	49.9	48.0	45.3	49.5	39.9
σ-Rittmann	4.65	4.64	4.46	4.69	4.38	4.51	4.55	4.66	4.75	4.36	4.77
A/CNK	0.86	0.85	0.90	0.90	0.87	0.91	0.88	0.87	0.86	1.00	0.85
A/NK	1.07	1.03	1.08	1.05	1.08	1.07	1.06	1.08	1.03	1.09	1.08
Li	55.3	57.0	56.3	62.6	56.1	54.2	49.7	49.3	41.9	40.8	61.0
Be	12.0	11.1	13.4	13.5	10.8	10.1	12.5	10.4	10.9	10.7	9.59
Sc	4.49	4.30	4.57	5.35	4.60	4.05	5.82	4.65	4.86	4.15	3.78
V	49.7	42.3	52.3	56.1	46.7	41.5	47.3	37.7	40.1	36.7	44.8
Cr	14.3	16.0	15.1	17.6	13.5	12.7	18.4	10.2	12.0	12.6	13.2
Co	4.26	4.69	4.44	5.12	4.18	3.50	4.61	3.63	3.91	3.89	3.83
Ni	11.0	13.2	11.0	13.7	10.0	8.8	12.5	8.1	8.5	9.8	10.1
Cu	12.6	7.9	17.7	9.3	8.9	3.9	23.3	8.9	7.9	12.6	8.8
Zn	125	91	115	148	106	75	119	78	69	77	152
Ga	29.4	28.5	31.8	32.6	28.7	28.3	32.2	28.6	31.0	28.4	28.5
Rb	326	336	388	382	315	343	340	335	380	313	315
Sr	932	844	979	915	864	829	1012	675	872	723	592
Zr	141	140	144	150	130	116	151	120	122	133	118
Nb	16.2	16.0	17.4	18.5	15.7	14.6	17.2	14.7	16.0	15.2	15.2
Cs	7.42	9.75	11.00	14.80	8.71	9.84	8.81	12.00	13.50	8.80	8.18
Ba	1592	1546	1609	1854	1453	1466	1671	1366	1589	1412	1313
Hf	4.82	4.75	4.79	5.07	4.44	4.04	4.93	4.22	4.37	4.38	4.11
Ta	0.983	1.010	1.050	1.120	0.939	0.938	1.060	0.924	0.985	0.938	0.894
Pb	174	196	182	201	226	94	252	93	110	118	177
Th	60.3	58.7	62.2	60.2	55.0	54.8	60.3	56.3	58.8	54.7	58.1
U	10.9	10.6	11.5	10.3	11.1	9.4	11.7	11.2	10.3	10.6	8.9
La	84.5	83.0	93.4	98.3	82.5	80.2	95.4	78.4	82.4	82.9	66.3
Ce	144	143	155	165	139	133	156	132	139	138	118
Pr	18.1	18.5	19.9	21.2	17.5	16.6	20.0	16.6	17.5	17.3	15.5
Nd	68.8	66.1	72.4	78.2	66.1	59.9	72.3	62.1	64.6	63.8	58.3
Sm	10.7	11.1	11.8	12.3	10.5	9.8	12.0	10.2	10.7	10.3	9.3
Eu	2.17	2.22	2.34	2.46	2.09	1.97	2.39	2.05	2.14	1.97	1.96
Gd	7.19	7.10	7.69	8.07	6.73	6.49	7.86	6.56	6.94	6.65	6.27
Tb	0.869	0.845	0.921	0.980	0.810	0.761	0.909	0.782	0.827	0.816	0.771
Dy	3.44	3.51	3.75	4.03	3.23	3.09	3.73	3.06	3.33	3.27	3.16
Ho	0.466	0.469	0.490	0.518	0.424	0.408	0.484	0.422	0.460	0.420	0.419
Er	1.28	1.26	1.36	1.43	1.23	1.13	1.39	1.19	1.28	1.18	1.14
Tm	0.160	0.163	0.169	0.182	0.147	0.138	0.169	0.145	0.168	0.154	0.158
Yb	0.898	0.885	1.000	1.050	0.887	0.828	0.978	0.864	0.954	0.851	0.876
Lu	0.128	0.126	0.147	0.151	0.118	0.116	0.138	0.112	0.125	0.121	0.122
Y	13.7	13.7	14.8	16.1	13.4	12.7	15.2	13.3	13.9	12.7	13.0
ΣREE	356.4	352.0	385.2	410.0	344.7	327.1	389.0	327.8	344.3	340.4	295.3
LREE/HREE	11.7	11.5	11.7	11.6	11.8	11.8	11.6	11.4	11.3	12.0	10.4
δEu	0.71	0.71	0.70	0.71	0.71	0.71	0.71	0.72	0.71	0.68	0.74
$(La/Yb)_N$	67.5	67.3	67.0	67.2	66.7	69.5	70.0	65.1	62.0	69.9	54.3

续表 3

Continued Table 3

样品号	PCL09-1-23	PCL09-1-24	PCL09-1-25	PCL09-2-1	PCL09-2-2	PCL09-2-3	PCL09-2-4	PCL09-2-5	PCL09-2-8	PCL09-2-9	PCL09-2-10
SiO_2	67.44	67.50	67.83	68.85	68.87	69.96	69.59	69.79	69.59	69.47	68.99
TiO_2	0.32	0.31	0.29	0.28	0.23	0.22	0.23	0.23	0.22	0.25	0.26
Al_2O_3	14.57	14.75	14.77	15.12	15.24	14.99	15.13	14.84	14.93	14.94	15.01
$Fe_2O_3^T$	2.03	1.96	1.79	1.91	1.72	1.55	1.70	1.74	1.61	1.78	1.92
FeO	1.20	1.20	1.05	1.55	1.25	0.50	0.40	0.70	0.60	0.65	0.65
MnO	0.038	0.041	0.033	0.042	0.050	0.049	0.050	0.052	0.050	0.045	0.046
MgO	1.05	1.03	0.80	0.76	0.62	0.48	0.49	0.50	0.47	0.60	0.61
CaO	1.93	1.73	1.62	1.36	1.24	0.98	0.85	1.12	1.28	1.34	1.31
Na_2O	3.98	4.12	4.17	4.37	4.57	4.75	4.59	4.64	4.70	4.54	4.42
K_2O	6.62	6.40	6.43	6.40	6.28	6.05	6.29	6.18	6.16	6.21	6.41
P_2O_5	0.23	0.24	0.20	0.21	0.16	0.13	0.14	0.15	0.13	0.18	0.17
LOI	1.74	1.85	2.00	0.69	0.99	0.81	0.91	0.71	0.81	0.62	0.79
Total	99.81	99.80	99.82	99.82	99.83	99.91	99.93	99.87	99.88	99.90	99.86
K_2O/Na_2O	1.66	1.55	1.54	1.46	1.37	1.27	1.37	1.33	1.31	1.37	1.45
$Mg^{\#}$	50.6	51.0	47.0	44.1	41.7	38.0	36.4	36.3	36.6	40.0	38.6
σ-Rittmann	4.60	4.52	4.53	4.49	4.55	4.33	4.45	4.37	4.44	4.37	4.51
A/CNK	0.85	0.88	0.88	0.91	0.92	0.93	0.95	0.91	0.89	0.90	0.90
A/NK	1.06	1.07	1.07	1.07	1.06	1.04	1.05	1.03	1.04	1.05	1.06
Li	39.8	48.1	57.4	42.7	28.3	29.3	26.2	28.6	35.7	45.5	40.2
Be	12.6	11.0	11.0	11.1	10.2	11.3	10.8	11.0	11.9	13.0	10.8
Sc	4.40	4.03	3.96	4.03	3.05	3.07	3.54	3.04	3.20	4.39	3.75
V	41.4	38.2	59.0	39.6	34.4	32.8	42.5	32.0	29.6	43.4	56.5
Cr	14.3	11.4	12.9	20.5	14.0	9.27	12.1	10.3	9.3	16.9	18.2
Co	4.35	3.87	3.37	4.27	3.62	2.61	2.74	2.78	2.60	3.83	3.81
Ni	11.7	8.6	7.4	11.6	7.0	3.8	4.5	4.0	3.7	9.4	8.9
Cu	13.2	13.4	9.4	8.8	17.8	2.4	3.6	5.2	5.8	3.1	6.1
Zn	84	72	84	82	99	96	101	99	96	84	88
Ga	31.9	28.6	29.8	29.7	30.1	31.2	30.9	30.5	32.5	35.5	32.2
Rb	339	340	341	343	327	348	341	348	373	372	342
Sr	859	704	719	1037	874	808	809	867	890	1071	1024
Zr	144	127	116	125	84	80	85	81	82	122	108
Nb	16.6	15.1	15.0	15.0	13.0	13.5	13.5	13.2	13.7	16.2	14.6
Cs	9.31	9.62	9.68	8.77	10.40	10.70	10.50	10.00	10.70	10.50	10.30
Ba	1558	1339	1411	1767	1431	1357	1405	1341	1429	1647	1626
Hf	4.90	4.27	4.04	4.23	3.03	3.04	3.16	3.05	3.13	4.28	3.63
Ta	1.040	0.934	0.906	0.940	0.816	0.865	0.860	0.863	0.896	1.020	0.909
Pb	120	109	128	101	136	124	138	101	148	124	129
Th	58.1	55.9	52.2	55.6	46.2	48.7	51.4	53.1	58.3	60.2	59.3
U	11.1	10.0	10.2	9.4	8.1	8.7	8.2	8.4	9.5	9.6	9.7
La	90.5	79.6	78.5	85.2	76.7	72.8	79.9	78.8	82.8	97.6	83.5
Ce	148	134	127	142	123	122	129	127	133	157	138
Pr	18.7	17.0	15.9	17.9	14.8	14.5	15.6	15.2	15.7	19.1	16.7
Nd	68.8	63.4	59.0	64.8	52.6	51.6	55.0	54.9	56.1	68.3	61.1
Sm	11.1	10.4	9.5	10.8	8.7	8.6	9.0	8.8	9.1	10.6	9.8
Eu	2.28	2.02	1.95	2.26	1.81	1.77	1.88	1.76	1.85	2.12	2.00
Gd	7.29	6.76	6.41	7.00	5.94	5.83	6.08	5.92	6.19	7.37	6.62
Tb	0.868	0.786	0.762	0.831	0.718	0.707	0.703	0.704	0.726	0.890	0.812
Dy	3.66	3.22	3.12	3.47	2.89	2.92	2.87	2.85	2.99	3.62	3.25
Ho	0.462	0.425	0.415	0.455	0.359	0.373	0.374	0.378	0.395	0.457	0.405
Er	1.34	1.18	1.13	1.22	0.97	0.97	1.02	1.05	1.10	1.25	1.16
Tm	0.169	0.149	0.148	0.150	0.116	0.132	0.133	0.135	0.135	0.163	0.135
Yb	0.974	0.833	0.854	0.889	0.723	0.707	0.752	0.759	0.753	0.899	0.780
Lu	0.133	0.117	0.114	0.119	0.099	0.097	0.104	0.091	0.098	0.128	0.113
Y	14.3	13.4	12.8	13.7	11.6	11.7	11.9	11.7	12.3	14.4	12.8
ΣREE	368.6	333.3	317.6	350.8	301.0	294.7	314.3	310.0	323.2	383.9	337.2
LREE/HREE	11.6	11.4	11.3	11.6	11.9	11.6	12.1	12.1	12.1	12.2	11.9
δEu	0.73	0.69	0.72	0.74	0.73	0.72	0.73	0.70	0.71	0.70	0.72
$(La/Yb)_N$	66.7	68.5	65.9	68.7	76.1	73.9	76.2	74.5	78.9	77.9	76.8

注:$Mg^{\#} = Mg^{2+}/(Mg^{2+} + Fe^{2+})$;$\sigma$-Rittmann = $(K_2O + Na_2O)^2/(SiO_2 - 43)$;A/CNK = $Al_2O_3/(CaO + Na_2O + K_2O)$,分子数比;A/NK = $Al_2O_3/(Na_2O + K_2O)$,分子数比;$(La/Yb)_N$ 是球粒陨石标准化(Sun and McDonough, 1989)后的比值;$\delta Eu = 2 \times (Eu)_N/((Sm)_N + (Gd)_N)$

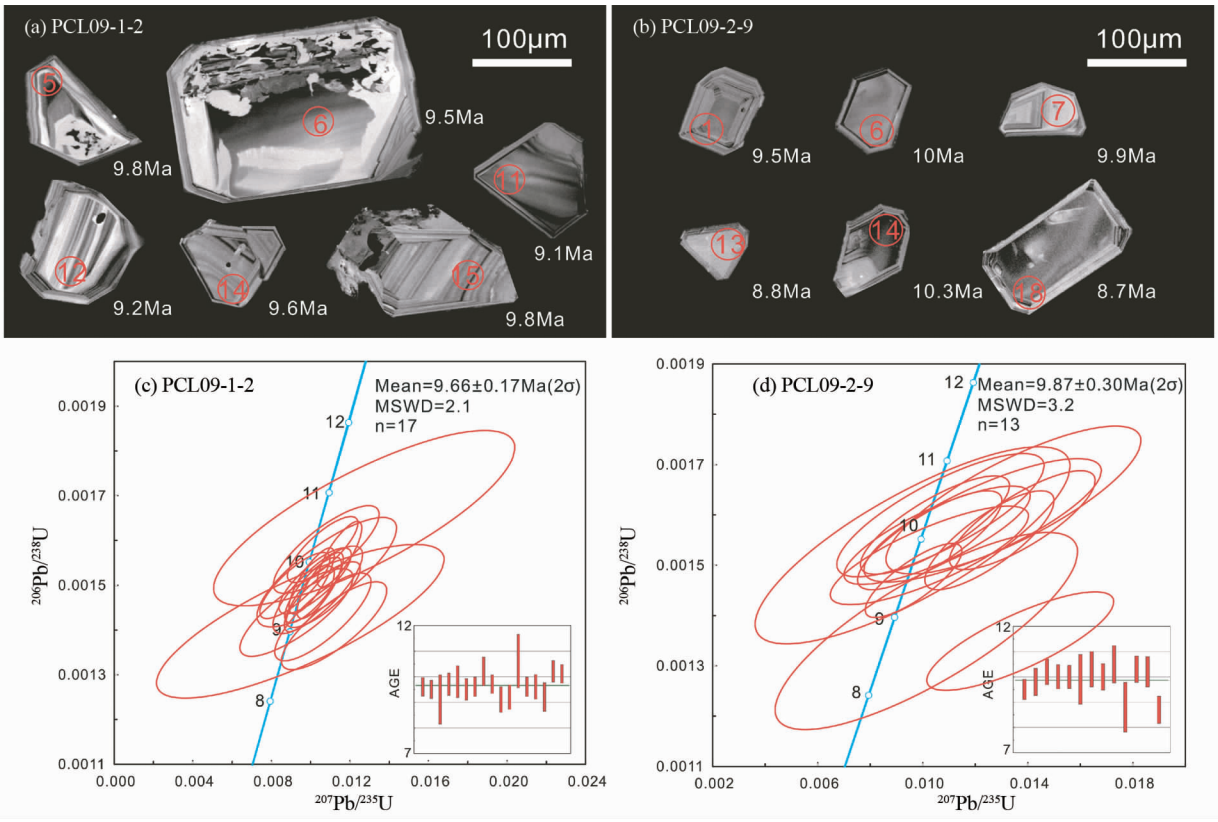

图 3 藏南彭措林岩脉锆石 CL 图像(a、b)与 U-Pb 年龄(c、d)

Fig. 3 Cathodoluminescene images (a, b) and U-Pb ages (c, d) for zircons from dykes in Pengcuolin, southern Tibet

表 4 藏南彭措林岩脉 Sr-Nd-Pb 同位素组成

Table 4 Sr-Nd-Pb isotopic compositions from dykes in Pengcuolin, southern Tibet

样品号	PCL09-1-5	PCL09-1-19	PCL09-1-23	PCL09-2-1	PCL09-2-5
Sm ($\times10^{-6}$)	12.3	10.2	11.1	10.8	8.8
Nd ($\times10^{-6}$)	78.2	62.1	68.8	64.8	54.9
$^{147}Sm/^{144}Nd$	0.0950	0.0992	0.0975	0.1007	0.0966
$^{143}Nd/^{144}Nd$	0.512093	0.512131	0.512072	0.512087	0.512081
$\pm2\sigma$	0.000007	0.000007	0.000010	0.000010	0.000010
Rb ($\times10^{-6}$)	382	335	339	343	348
Sr ($\times10^{-6}$)	915	675	859	1037	867
$^{87}Rb/^{86}Sr$	1.2080	1.4361	1.1419	0.9571	1.1614
$^{87}Sr/^{86}Sr$	0.712337	0.712168	0.712295	0.712400	0.712406
$\pm2\sigma$	0.000009	0.000009	0.000009	0.000012	0.000014
$(^{143}Nd/^{144}Nd)_i$	0.512087	0.512125	0.512066	0.512080	0.512075
$(^{87}Sr/^{86}Sr)_i$	0.712171	0.711971	0.712138	0.712266	0.712243
$\varepsilon_{Nd}(t)$	−10.51	−9.77	−10.92	−10.63	−10.74
t_{DM}(Ga)	1.36	1.36	1.41	1.43	1.39
$^{206}Pb/^{204}Pb$	18.829	18.839	18.844	18.841	18.837
2σ	0.001	0.001	0.002	0.002	0.004
$^{207}Pb/^{204}Pb$	15.728	15.708	15.709	15.713	15.724
2σ	0.001	0.001	0.001	0.002	0.003
$^{208}Pb/^{204}Pb$	39.523	39.456	39.459	39.471	39.511
2σ	0.003	0.004	0.003	0.004	0.007

注：$^{147}Sm/^{144}Nd$ 和 $^{87}Rb/^{86}Sr$ 比值采用 ICP-MS 测得的 Sm、Nd、Rb、Sr 含量计算得出；$(^{147}Sm/^{144}Nd)_{DM}=0.2137$，$(^{143}Nd/^{144}Nd)_{DM}=0.51315$（Peucat *et al.*, 1989）；$(^{147}Sm/^{144}Nd)_{CHUR}=0.1967$（Jacobsen and Wasserburg, 1980）；$(^{143}Nd/^{144}Nd)_{CHUR}=0.512638$（Goldstein *et al.*, 1984）

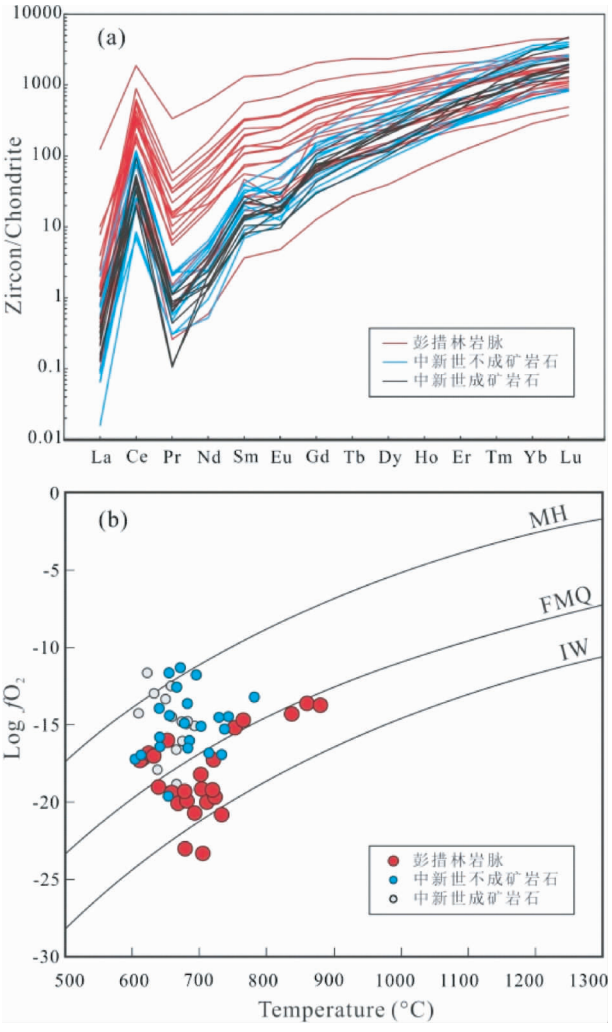

图 4 藏南彭措林岩脉锆石球粒陨石标准化 REE 图解(a,标准化值据 Sun and McDonough, 1989)和温度-氧逸度关系图(b,据 Qiu *et al.*, 2013)

冈底斯斑岩铜矿带中新世不成矿岩石和成矿岩石的数据来自 Wang *et al.* (2014a, b), Yang *et al.* (2016, unpub. data)

Fig. 4 Chondrite-normalized REE parterns (a, normalization values after Sun and McDonough, 1989) and oxygen fugacity (b, after Qiu *et al.*, 2013) for zircons from dykes in Pengcuolin, southern Tibet

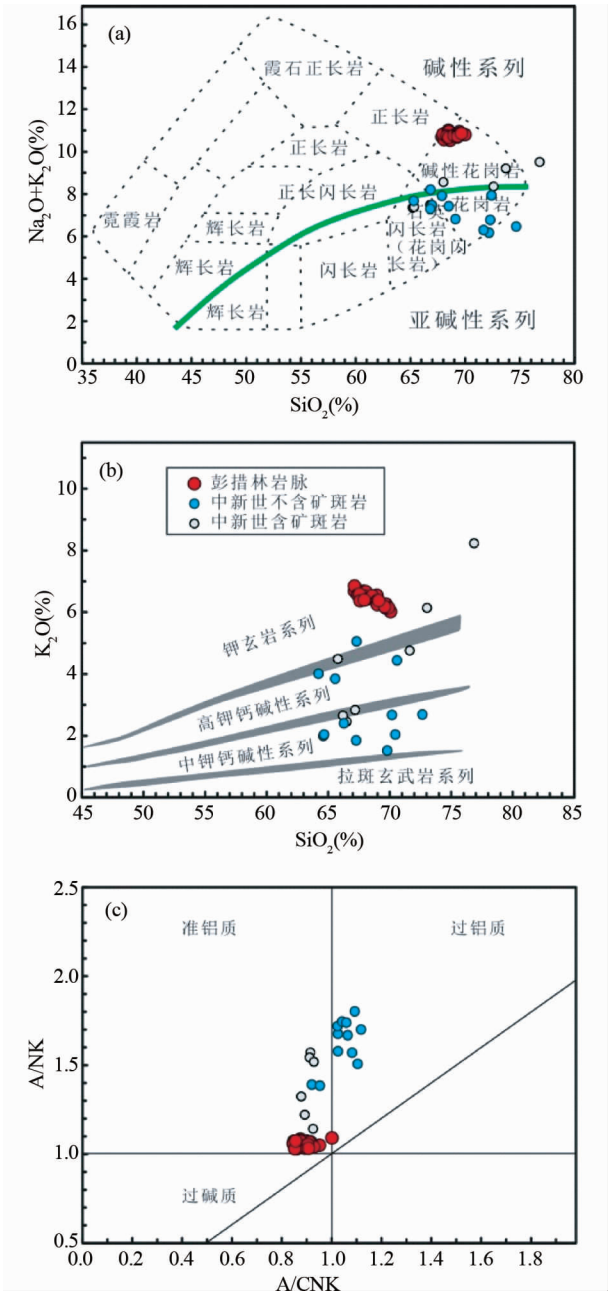

图 5 藏南彭措林岩脉主量元素分类图解

(a)侵入岩分类图解(Wilson, 1989);(b) K_2O-SiO_2 分类图解(Rickwood, 1989);(c) A/NK-A/CNK 分类图解. 冈底斯埃达克质不含矿斑岩和含矿斑岩数据来自 Hou *et al.* (2013)

Fig. 5 Diagrams of dykes in Pengcuolin, southern Tibet

(a) classification diagram of intrusive rock (Wilson, 1989), the line between alkaline and subalkalines series after Irvine and Baragar (1971); (b) K_2O-SiO_2 diagram (Rickwood, 1989); (c) A/NK-A/CNK diagram

据全岩主量地球化学特征可知(图 5),彭措林岩脉属于钾玄岩系列、准铝质碱性花岗岩。

4.3 全岩微量元素

彭措林岩脉稀土元素总含量 $\Sigma REE = 294.7 \times 10^{-6} \sim 410.0 \times 10^{-6}$,轻重稀土分异明显(LREE/HREE = 10.4 ~ 12.2, $(La/Yb)_N = 54 \sim 79$),显示富集轻稀土元素(LREE)、亏损重稀土元素(HREE)及弱 Eu 负异常($\delta Eu = 0.68 \sim 0.74$)的特征(图 6a)。同时,彭措林岩脉强烈富集 Th、U、Pb 等大离子亲石元素(LILE),强烈亏损 Nb、Ta、P、Ti 等高场强元素(HFSE)(图 6b)。

此外,在微量元素特征上,相容元素 Cr、Ni 含量较低(Cr

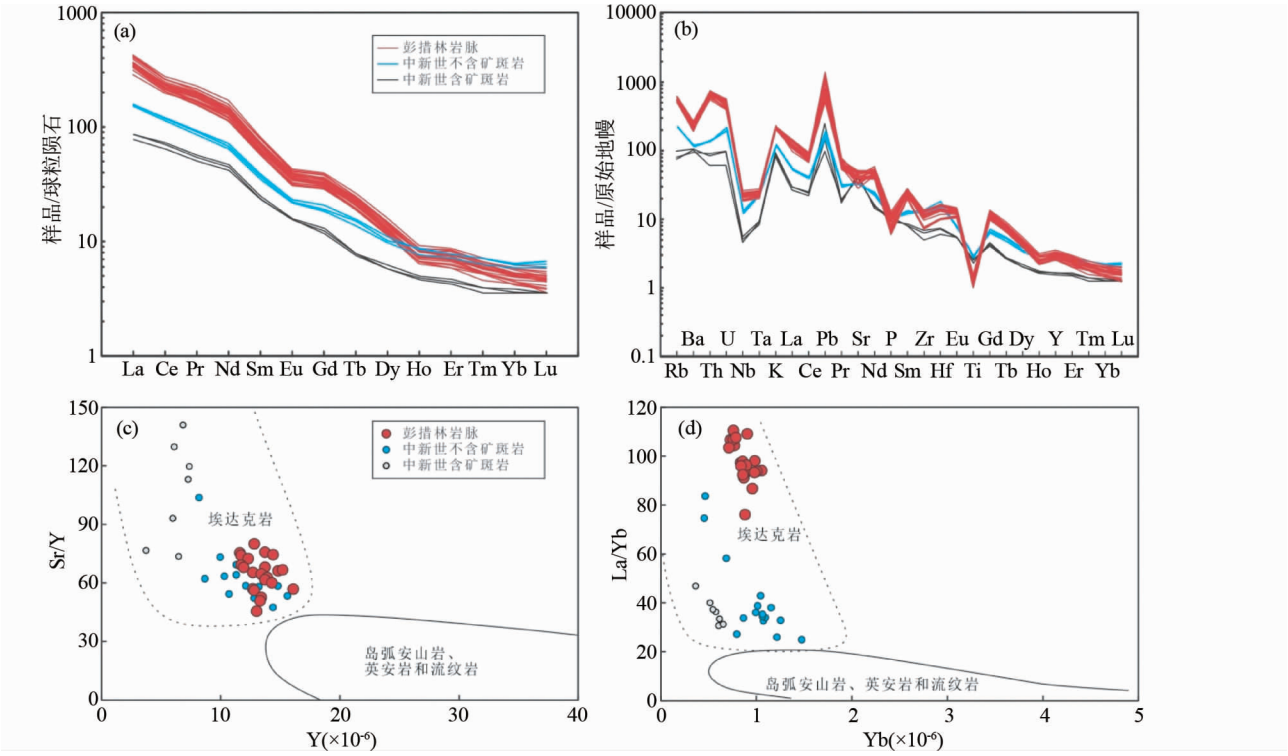

图 6 藏南彭措林岩脉微量元素图解

(a)球粒陨石标准化稀土元素配分图;(b)原始地幔标准化微量元素蛛网图(a、b,标准化值据 Sun and McDonough, 1989);(c) Sr/Y-Y (Defant and Drummond, 1990);(d) La/Yb-Yb(Richards and Kerrich, 2007; Castillo, 2012). 冈底斯埃达克质不含矿斑岩和含矿斑岩微量数据来自 Hou *et al.* (2013)

Fig. 6 Plots of dykes in Pengcuolin, southern Tibet

(a) chondrite-normalized REE patterns; (b) primitive mantle normalized multi-element diagrams (a, b, normalization values after Sun and McDonough, 1989); (c) Sr/Y vs. Y (Defant and Drummond, 1990); (d) La/Yb vs. Yb (Richards and Kerrich, 2007; Castillo, 2012)

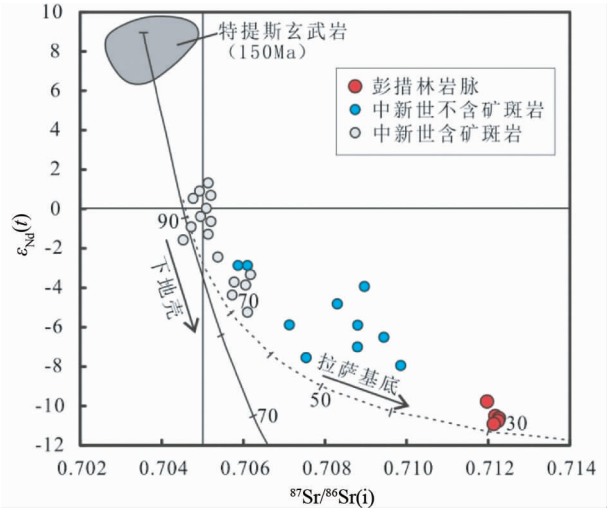

图 7 藏南彭措林岩脉 ε_{Nd}-$^{87}Sr/^{86}Sr$ 图解(据 Hou *et al.*, 2013; Zheng *et al.*, 2014 改绘)

冈底斯埃达克质含矿斑岩和不含矿斑岩数据来自 Hou *et al.* (2013)

Fig. 7 ε_{Nd} vs. $^{87}Sr/^{86}Sr$ plot for dykes in Pengcuolin, southern Tibet (modified after Hou *et al.*, 2013; Zheng *et al.*, 2014)

$=9.27\times10^{-6}\sim20.5\times10^{-6}$, Ni $=3.7\times10^{-6}\sim13.7\times10^{-6}$; 表 3);Nb/Ta 比值较高(15.3 ~ 17.0);具有高 Sr/Y 和 La/Yb 比值、低 Y 和 Yb 值的典型埃达克质地球化学特征(Sr/Y = 45.5 ~ 80.0, La/Yb = 75.7 ~ 110, Y $=11.6\times10^{-6}\sim16.1\times10^{-6}$, Yb $=0.7\times10^{-6}\sim1.1\times10^{-6}$; 图 6c, d)。

4.4 Sr-Nd-Pb 同位素

彭措林岩脉 5 件样品的 Sr、Nd 同位素比值变化范围较小,$^{87}Sr/^{86}Sr_{(i)}=0.7120\sim0.7123$, $^{143}Nd/^{144}Nd_{(i)}=0.51207\sim0.51213$;$\varepsilon_{Nd}(t)$ 介于 −10.92 ~ −9.77 之间,平均值为 −10.51(图 7);Nd 同位素亏损地幔模式年龄在 1.36 ~ 1.43Ga 之间。彭措林岩脉 6 件样品的 Pb 同位素比值较高($^{206}Pb/^{204}Pb=18.812\sim18.844$, $^{207}Pb/^{204}Pb=15.705\sim15.728$, $^{208}Pb/^{204}Pb=39.424\sim39.523$),变化范围较小,分布于北半球参考线(NHRL)之上、地球等时线(Geochron)右侧(图 8)。

5 讨论

5.1 岩石成因与岩浆源区

与区域上广泛分布的中新世冈底斯后碰撞埃达克质岩

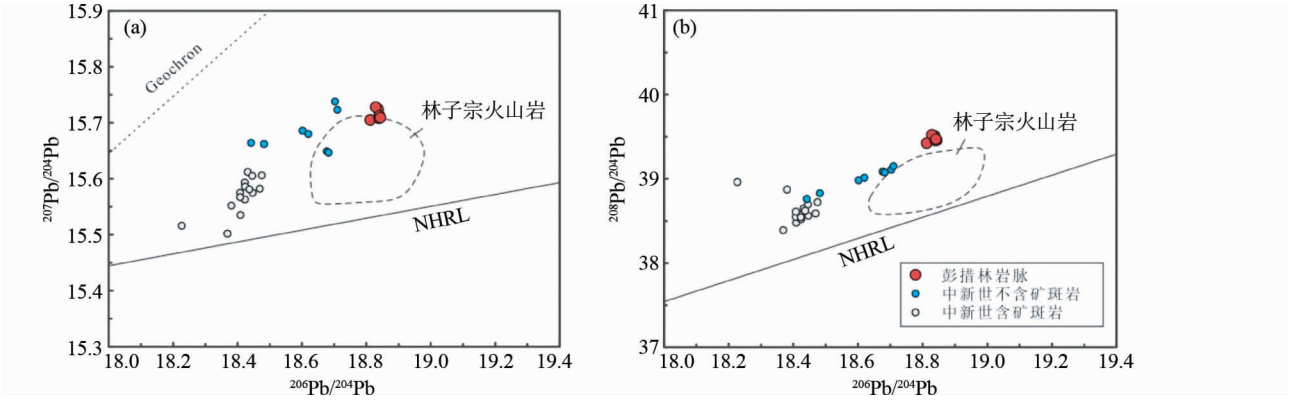

图 8 藏南彭措林岩脉$^{207}Pb/^{204}Pb$-$^{206}Pb/^{204}Pb$及$^{208}Pb/^{204}Pb$-$^{206}Pb/^{204}Pb$同位素比值图解

冈底斯埃达克质不含矿斑岩数据来自 Gao *et al.* (2010);冈底斯埃达克质含矿斑岩数据来自 Hou *et al.* (2004);林子宗火山岩区域来自 Mo *et al.* (2007)

Fig. 8 Plots of $^{207}Pb/^{204}Pb$ and $^{208}Pb/^{204}Pb$ vs. $^{206}Pb/^{204}Pb$ showing the Pb isotopic compositions for dykes in Pengcuolin, southern Tibet

浆一样,彭措林岩脉具有高 Sr/Y 和 La/Yb 比值、低 Y 和 Yb 值的典型埃达克质地球化学属性(Sr/Y = 45.5 ~ 80.0, La/Yb = 75.7 ~ 110.0, Y = 11.6 × 10^{-6} ~ 16.1 × 10^{-6}, Yb = 0.7 × 10^{-6} ~ 1.1 × 10^{-6}; 图 6c, d)。关于冈底斯后碰撞埃达克质岩浆的成因,有如下解释:(1)俯冲过程中受改造的陆下岩石圈地幔的熔融(Gao *et al.*, 2007, 2010; Richards, 2009);(2)加厚古老下地壳的熔融(Chung *et al.*, 2003; Xu *et al.*, 2010);(3)加厚新生镁铁质下地壳的熔融(Hou *et al.*, 2004; Chung *et al.*, 2009; Li *et al.*, 2011; 秦克章等, 2014)。

在主微量元素上,彭措林埃达克质岩脉具有低 MgO、Cr、Ni 和 $Mg^{\#}$的特征,与幔源熔体的组成特征不一致,排除了其起源于岩石圈地幔熔融的可能性(Wang *et al.*, 2008; Xu *et al.*, 2010)。同时,彭措林岩脉亏损重稀土元素和 Y,这需要来自石榴子石稳定区域(对应深度≥50km 的榴辉岩相或角闪-榴辉岩相)的镁铁质岩石的部分熔融(Rapp *et al.*, 1999; Xiong, 2006),意味着其源区可能为加厚的下地壳(Atherton and Petford, 1993; Chung *et al.*, 2003; Hou *et al.*, 2004; Xu *et al.*, 2010)。此外,从 Sr-Nd 同位素特征上来看,相较于西藏中新世冈底斯埃达克质含矿斑岩起源于加厚新生镁铁质下地壳的熔融($\varepsilon_{Nd}(t)$ = −6.2 ~ 2.2; Zheng *et al.*, 2012a, b; Hou *et al.*, 2013; Yang *et al.*, 2015),彭措林岩脉($\varepsilon_{Nd}(t)$ = −10.9 ~ −9.8)和中新世不含矿斑岩($\varepsilon_{Nd}(t)$ = −8.1 ~ −3.0; Hou *et al.*, 2013)则同样具有更低的 $\varepsilon_{Nd}(t)$值,指示其起源于加厚古老下地壳的熔融。通过进一步比较彭措林岩脉与西藏古老下地壳的$^{87}Sr/^{86}Sr_{(i)}$比值可知,彭措林岩脉很有可能起源于西藏古老下地壳($^{87}Sr/^{86}Sr_{(i)}$ > 0.706, $\varepsilon_{Nd}(t)$ < −3; Hou *et al.*, 2013)。主微量元素和 Sr-Nd 同位素特征共同表明,彭措林岩脉很可能起源于加厚的拉萨下地壳,在其形成过程中有较少幔源物质的加入。

同时,通过锆石 Ce 异常和 Ti 温度计算(Blundy and Wood, 1994; Watson and Harrison, 2005; Qiu *et al.*, 2013; Trail *et al.*, 2011, 2012),彭措林岩脉的氧逸度范围为 −23.4 ~ −13.6, ΔFMQ = −6.7 ~ +2.1(平均值为 −1.4)(图 4b),表明该岩脉的氧逸度较低,进而指示其岩浆源区氧逸度也较低。经由同样的方法计算可知,在冈底斯斑岩铜矿带(89°E ~ 93°E),中新世不成矿岩石的氧逸度范围为 −19.6 ~ −11.3, ΔFMQ = −1.6 ~ +6.4(平均值为 2.4);成矿岩石的氧逸度范围为 −18.9 ~ −11.7, ΔFMQ = −1.1 ~ +7.3(平均值为 3.1)(图 4b, Wang *et al.*, 2014a, b; Yang *et al.*, 2016; Yang *et al.*, unpub. data)。通过对比可知,在岩浆源区氧逸度上,彭措林岩脉岩浆源区的氧逸度均低于中新世不成矿岩石和成矿岩石岩浆源区的氧逸度。

与冈底斯埃达克质含矿斑岩(Hou *et al.*, 2004, 2013)、不含矿斑岩(Gao *et al.*, 2010; Hou *et al.*, 2013)进行综合对比可知,彭措林岩脉与含矿斑岩、不含矿斑岩均具有明显的埃达克质属性(图 6c, d);较含矿斑岩和不含矿斑岩具有更高的$^{87}Sr/^{86}Sr_{(i)}$比值、更低的 $\varepsilon_{Nd}(t)$值、更高的 Pb 同位素比值(图 7、图 8)。在岩浆源区上,彭措林岩脉与冈底斯斑岩铜矿带中新世不含矿斑岩具有一致性,即起源于加厚的、新生幔源组分有限的、低氧逸度的古老下地壳。

5.2 对区域成矿作用的启示

最近的研究表明,冈底斯斑岩铜矿带的含矿斑岩来自于下地壳富含硫化物堆晶体的重熔(Hou *et al.*, 2015a),该新生下地壳(堆晶体)形成于中生代特提斯洋的俯冲过程,其机制类似于环太平洋弧岩浆带(Lee *et al.*, 2012; Chiaradia, 2014)。然而,彭措林岩脉岩浆源区下地壳中新生幔源组分十分有限,指示了古老下地壳中岛弧幔源岩浆注入量较少,因而岛弧期堆晶至下地壳的金属硫化物含量极为有限,故而不利于形成含矿斑岩。另外,斑岩型矿床的形成,同时要求

岩浆具有高氧逸度。在硅酸盐熔体中,硫在高氧逸度条件下以硫酸根的形式溶解于岩浆之中,促使通常优先向硫化物分配的 Cu、Au 等作为不相容元素向熔体中富集(Hamlyn *et al.*, 1985; Bornhorst and Rose Jr, 1986; Richards *et al.*, 1991; Richards, 1995; Jugo *et al.*, 2005)。由于彭措林岩脉是低氧逸度的,所以即使其岩浆源区有足够的金属硫化物存在,如此低氧逸度的岩浆也无法将源区的硫化物有效萃取,因而低氧逸度也制约了其成矿潜力。由此可知,并非冈底斯成矿带所有的埃达克岩都具有成矿潜力,而应具体分析其岩浆源区的特征,从幔源贡献率和氧逸度来评价其成矿潜力。

另外,已有研究表明,拉萨地体的地壳基底存在大区域尺度上的不均一性(Zhu *et al.*, 2011; Hou *et al.*, 2015b)。从 Hf 同位素填图上可知,北拉萨地体 90°E 以东为古老物质,中拉萨地体几乎均为古老物质,南拉萨地体 83°E ~ 87°E 之间为古老物质(Hou *et al.*, 2015b)。然而,在彭措林西北方向 59km 处发育的朱诺斑岩 Cu-Mo 矿床(87°28′E),其含矿斑岩成岩年龄为 15.6Ma、成矿年龄为 13.7Ma(郑有业等, 2007);其花岗岩岩体具有富集的 Hf 同位素($\varepsilon_{Hf}(t)$ = -9.87 ~ 0.21)特征并具有古老二阶段模式年龄(1.08 ~ 1.73Ga),壳源贡献率达 30.5% ~ 33.4%,反映出矿区中新世岩浆岩的古老下地壳混染程度较高,可能指示古老拉萨地体的印迹(黄勇等, 2015)。同时,起源于古老下地壳的彭措林岩脉(88°E)的存在,也进一步表明在南拉萨地体 87°E 以东的新生下地壳中存在西藏古老下地壳物质,暗示拉萨地体地壳基底组成的不均一性在小区域范围内也有所显示。

6 结论

(1)彭措林岩脉形成于 ~ 10Ma,较中新世冈底斯斑岩铜矿带中段含矿斑岩的年龄更新,表明该时期的埃达克质岩浆作用可能一直持续到了 10Ma 左右。

(2)彭措林岩脉为钾玄岩系列、准铝质碱性花岗岩;轻重稀土分异明显(LREE/HREE = 10.4 ~ 12.2, $(La/Yb)_N$ = 54 ~ 79),存在弱 Eu 负异常(δEu = 0.68 ~ 0.74);强烈富集大离子亲石元素,强烈亏损高场强元素;具有高 Sr/Y 和 La/Yb 比值、低 Y 和 Yb 值的典型埃达克质地球化学特征;高 $^{87}Sr/^{86}Sr_{(i)}$ 比值和低 $\varepsilon_{Nd}(t)$ 值($^{87}Sr/^{86}Sr_{(i)}$ = 0.7120 ~ 0.7123, $\varepsilon_{Nd}(t)$ = -10.9 ~ -9.8),暗示其可能起源于加厚的古老拉萨地体下地壳的部分熔融。

(3)彭措林岩脉下地壳岩浆源区中新生幔源组分含量较少,指示了古老下地壳中岛弧幔源岩浆注入量较少,因而岛弧期堆晶至下地壳的金属硫化物量极为有限,加之氧逸度较低导致岩浆萃取金属的能力也相对较弱,故而彭措林埃达克质岩脉不具备成矿潜力。

致谢 感谢中国科学院地球化学研究所罗泰义研究员在野外工作中的帮助和指导!感谢西北大学大陆动力学国家重点实验室以及核工业北京地质研究院分析测试研究中心的老师和同学在测试工作中的帮助和指导!感谢团队曹康博士、李秋耘博士在文章修改阶段的帮助!感谢两位匿名审稿专家对本文提出的宝贵评审意见!

References

Andersen T. 2002. Correction of common lead in U-Pb analyses that do not report ^{204}Pb. Chemical Geology, 192(1-2): 59-79

Atherton MP and Petford N. 1993. Generation of sodium-rich magmas from newly underplated basaltic crust. Nature, 362(6416): 144-146

Blundy J and Wood B. 1994. Prediction of crystal-melt partition coefficients from elastic moduli. Nature, 372(6505): 452-454

Bornhorst TJ and Rose Jr WI. 1986. Partitioning of gold in young calc-alkalic volcanic rocks from Guatemala. The Journal of Geology, 94(3): 412-418

Castillo PR. 2012. Adakite petrogenesis. Lithos, 134-135: 304-316

Chiaradia M. 2014. Copper enrichment in arc magmas controlled by overriding plate thickness. Nature Geoscience, 7(1): 43-46

Chung SL, Liu DY, Ji JQ, Chu MF, Lee HY, Wen DJ, Lo CH, Lee TY, Qian Q and Zhang Q. 2003. Adakites from continental collision zones: Melting of thickened lower crust beneath southern Tibet. Geology, 31(11): 1021-1024

Chung SL, Chu MF, Ji JQ, O'Reilly SY, Pearson NJ, Liu DY, Lee TY and Lo CH. 2009. The nature and timing of crustal thickening in Southern Tibet: Geochemical and zircon Hf isotopic constraints from postcollisional adakites. Tectonophysics, 477(1-2): 36-48

Defant MJ and Drummond MS. 1990. Derivation of some modern arc magmas by melting of young subducted lithosphere. Nature, 347(6294): 662-665

Gao YF, Hou ZQ, Kamber BS, Wei RH, Meng XJ and Zhao RS. 2007. Adakite-like porphyries from the southern Tibetan continental collision zones: Evidence for slab melt metasomatism. Contributions to Mineralogy and Petrology, 153(1): 105-120

Gao YF, Yang ZS, Santosh M, Hou ZQ, Wei RH and Tian SH. 2010. Adakitic rocks from slab melt-modified mantle sources in the continental collision zone of southern Tibet. Lithos, 119(3-4): 651-663

Goldstein SL, O'Nions RK and Hamilton PJ. 1984. A Sm-Nd isotopic study of atmospheric dusts and particulates from major river systems. Earth and Planetary Science Letters, 70(2): 221-236

Hamlyn PR, Keays RR, Cameron WE, Crawford AJ and Waldron HM. 1985. Precious metals in magnesian low-Ti lavas: Implications for metallogenesis and sulfur saturation in primary magmas. Geochimica et Cosmochimica Acta, 49(8): 1797-1811

Hoskin PWO and Schaltegger U. 2003. The composition of zircon and igneous and metamorphic petrogenesis. Reviews in Mineralogy and Geochemistry, 53(1): 27-62

Hou ZQ, Qu XM, Huang W and Gao YF. 2001. Gangdise porphyry copper metallogenic belt: The possible second "Yulong" copper belt. Geology in China, 28(10): 27-29, 40 (in Chinese with English abstract)

Hou ZQ, Gao YF, Qu XM, Rui ZY and Mo XX. 2004. Origin of adakitic intrusives generated during Mid-Miocene east-west extension in southern Tibet. Earth and Planetary Science Letters, 220(1-2): 139-155

Hou ZQ, Qu XM, Wang SX, Gao YF, Du AD and Huang W. 2004. Re-Os age for molybdenite from the Gangdese porphyry copper belt on Tibetan Plateau: Implication for geodynamic setting and duration of the Cu mineralization. Science in China (Series D), 47(3): 221-231

Hou ZQ, Gao YF, Meng XJ, Qu XM and Huang W. 2004. Genesis of adakitic porphyry and tectonic controls on the Gangdese Miocene

porphyry copper belt in the Tibetan orogen. Acta Petrologica Sinica, 20(2): 239 – 248 (in Chinese with English abstract)

Hou ZQ, Qu XM, Yang ZS, Meng XJ, Li ZQ, Yang ZM, Zheng MP, Zheng YY, Nie FJ, Gao YF, Jiang SH and Li GM. 2006a. Metallogenesis in Tibetan collisional orogenic belt: III. Mineralization in post-collisional extension setting. Mineral Deposits, 25(6): 629 – 651 (in Chinese with English abstract)

Hou ZQ, Zhao ZD, Gao YF, Yang ZM and Jiang W. 2006b. Tearing and dischronal subduction of the Indian continental slab: Evidence from Cenozoic Gangdese volcano-magmatic rocks in South Tibet. Acta Petrologica Sinica, 22(4): 761 – 774 (in Chinese with English abstract)

Hou ZQ and Cook NJ. 2009. Metallogenesis of the Tibetan collisional orogen: A review and introduction to the special issue. Ore Geology Reviews, 36(1 – 3): 2 – 24

Hou ZQ, Zheng YC, Yang ZM and Yang ZS. 2012. Metallogenesis of continental collision setting: Part Ⅰ. Gangdese Cenozoic porphyry Cu-Mo systems in Tibet. Mineral Deposits, 31(4): 647 – 670 (in Chinese with English abstract)

Hou ZQ, Zheng YC, Yang ZM, Rui ZY, Zhao ZD, Jiang SH, Qu XM and Sun QZ. 2013. Contribution of mantle components within juvenile lower-crust to collisional zone porphyry Cu systems in Tibet. Mineralium Deposita, 48(2): 173 – 192

Hou ZQ, Duan LF, Lu YJ, Zheng YC, Zhu DC, Yang ZM, Yang ZS, Wang BD, Pei YR, Zhao ZD and McCuaig TC. 2015a. Lithospheric architecture of the Lhasa Terrane and its control on ore deposits in the Himalayan-Tibetan Orogen. Economic Geology, 110(6): 1541 – 1575

Hou ZQ, Yang ZM, Lu YJ, Kemp A, Zheng YC, Li QY, Tang JX, Yang ZS and Duan LF. 2015b. A genetic linkage between subduction- and collision-related porphyry Cu deposits in continental collision zones. Geology, 43(3): 247 – 250

Huang Y, Ding J, Li GM, Dai J, Yan GQ, Wang G and Liu XF. 2015. U-Pb dating, Hf isotopic characteristics of zircons from intrusions in the Zhuluo porphyry Cu-Mo-Au deposit and its mineralization significance. Acta Geologica Sinica, 89(1): 99 – 108 (in Chinese with English abstract)

Jacobsen SB and Wasserburg GJ. 1980. Sm-Nd isotopic evolution of chondrites. Earth and Planetary Science Letters, 50(1): 139 – 155

Jugo PJ, Luth RW and Richards JP. 2005. An experimental study of the sulfur content in basaltic melts saturated with immiscible sulfide or sulfate liquids at 1300℃ and 1.0GPa. Journal of Petrology, 46(4): 783 – 798

Lee CT, Luffi P, Chin EJ, Bouchet R, Dasgupta R, Morton DM, Roux VL, Yin QZ and Jin D. 2012. Copper systematics in arc magmas and implications for crust-mantle differentiation. Science, 336 (6077): 64 – 68

Li JX, Qin KZ, Li GM, Xiao B, Chen L and Zhao JX. 2011. Post-collisional ore-bearing adakitic porphyries from Gangdese porphyry copper belt, southern Tibet: Melting of thickened juvenile arc lower crust. Lithos, 126(3 – 4): 265 – 277

Liu D, Zhao ZD, Zhu DC, Niu YL, DePaolo DJ, Harrison TM, Mo XX, Dong GC, Zhou S, Sun CG, Zhang ZC and Liu JL. 2014. Postcollisional potassic and ultrapotassic rocks in southern Tibet: Mantle and crustal origins in response to India-Asia collision and convergence. Geochimica et Cosmochimica Acta, 143: 207 – 231

Ludwig KR. 2003. User's Manual for Isoplot/Ex, Version 3.00: A Geochronological Toolkit for Microsoft Excel. Berkeley, CA, USA: Berkeley Geochronology Center

Mo XX, Hou ZQ, Niu YL, Dong GC, Qu XM, Zhao ZD and Yang ZM. 2007. Mantle contributions to crustal thickening during continental collision: Evidence from Cenozoic igneous rocks in southern Tibet. Lithos, 96(1 – 2): 225 – 242

Peucat JJ, Vidal P, Bernard-Griffiths J and Condie KC. 1989. Sr, Nd, and Pb isotopic systematics in the Archean low- to high-grade transition zone of southern India: Syn-accretion vs. post-accretion granulites. The Journal of Geology, 97(5): 537 – 549

Qin KZ, Xia DX, Li GM, Xiao B, Duo J, Jiang GW and Zhao JX. 2014. Qulong Porphyry – Skarn Type Cu-Mo Deposit, Tibet. Beijing: Science Press, 1 – 316 (in Chinese)

Qiu JT, Yu XQ, Santosh M, Zhang DH, Chen SQ and Li PJ. 2013. Geochronology and magmatic oxygen fugacity of the Tongcun molybdenum deposit, Northwest Zhejiang, SE China. Mineralium Deposita, 48(5): 545 – 556

Qu XM, Hou ZQ, Zaw K and Li YG. 2007. Characteristics and genesis of Gangdese porphyry copper deposits in the southern Tibetan Plateau: Preliminary geochemical and geochronological results. Ore Geology Reviews, 31(1 – 4): 205 – 223

Rapp RP, Shimizu N, Norman MD and Applegate GS. 1999. Reaction between slab-derived melts and peridotite in the mantle wedge: Experimental constraints at 3.8GPa. Chemical Geology, 160(4): 335 – 356

Richards JP, McCulloch MT, Chappell BW and Kerrich R. 1991. Sources of metals in the Porgera gold deposit, Papua New Guinea: Evidence from alteration, isotope, and noble metal geochemistry. Geochimica et Cosmochimica Acta, 55(2): 565 – 580

Richards JP. 1995. Alkalic-type epithermal gold deposits: A review. In: Thompson JFH (ed.). Magmas, Fluids, and Ore Deposits. Mineralogical Association of Canada Short Course, 23: 367 – 400

Richards JP and Kerrich R. 2007. Special paper: Adakite-like rocks: Their diverse origins and questionable role in metallogenesis. Economic Geology, 102(4): 537 – 576

Richards JP. 2009. Postsubduction porphyry Cu-Au and epithermal Au deposits: Products of remelting of subduction-modified lithosphere. Geology, 37(3): 247 – 250

Rickwood PC. 1989. Boundary lines within petrologic diagrams which use oxides of major and minor elements. Lithos, 22(4): 247 – 263

Rui ZY, Li GM, Zhang LS and Wang LS. 2004. The response of porphyry copper deposits to important geological events in Xizang. Earth Science Frontiers, 11(1): 145 – 152 (in Chinese with English abstract)

Sillitoe RH. 1972. A plate tectonic model for the origin of porphyry copper deposits. Economic Geology, 67(2): 184 – 197

Sillitoe RH. 2010. Porphyry copper systems. Economic Geology, 105 (1): 3 – 41

Sun SS and McDonough WF. 1989. Chemical and isotopic systematics of oceanic basalts: Implications for mantle composition and processes. In: Saunders AD and Norry MJ (eds.). Magmatism in Ocean Basins. Geological Society, London, Special Publications, 42: 313 – 345

Trail D, Watson EB and Tailby ND. 2011. The oxidation state of Hadean magmas and implications for early Earth's atmosphere. Nature, 480 (7375): 79 – 82

Trail D, Watson EB and Tailby ND. 2012. Ce and Eu anomalies in zircon as proxies for the oxidation state of magmas. Geochimica et Cosmochimica Acta, 97: 70 – 87

Wang Q, Wyman DA, Xu JF, Dong YH, Vasconcelos PM, Pearson N, Wan YS, Dong H, Li CF, Yu YS, Zhu TX, Feng XT, Zhang QY, Zi F and Chu ZY. 2008. Eocene melting of subducting continental crust and early uplifting of central Tibet: Evidence from central-western Qiangtang high-K calc-alkaline andesites, dacites and rhyolites. Earth and Planetary Science Letters, 272(1 – 2): 158 – 171

Wang R, Richards JP, Hou ZQ, Yang ZM and DuFrane SA. 2014a. Increased magmatic water content: The key to Oligo-Miocene porphyry Cu-Mo ± Au formation in the eastern gangdese belt, Tibet. Economic Geology, 109(5): 1315 – 1339

Wang R, Richards JP, Hou ZQ, Yang ZM, Gou ZB and DuFrane SA. 2014b. Increasing magmatic oxidation state from Paleocene to Miocene in the eastern gangdese belt, Tibet: Implication for collision-related porphyry Cu-Mo ± Au mineralization. Economic Geology, 109(7): 1943 – 1965

Watson EB and Harrison TM. 2005. Zircon thermometer reveals minimum melting conditions on earliest Earth. Science, 308 (5723): 841 – 844

Wilson BM. 1989. Igneous Petrogenesis: A Global Tectonic Approach.

Netherlands: Springer
Xiong XL. 2006. Trace element evidence for growth of early continental crust by melting of rutile-bearing hydrous eclogite. Geology, 34(11): 945 – 948
Xu WC, Zhang HF, Guo L and Yuan HL. 2010. Miocene high Sr/Y magmatism, south Tibet: Product of partial melting of subducted Indian continental crust and its tectonic implication. Lithos, 114(3 – 4): 293 – 306
Yang ZM, Lu YJ, Hou ZQ and Chang ZS. 2015. High-Mg diorite from qulong in southern Tibet: Implications for the genesis of adakite-like intrusions and associated porphyry Cu deposits in collisional orogens. Journal of Petrology, 56(2): 227 – 254
Yang ZM, Hou ZQ, Chang ZS, Li QY, Liu YF, Qu HC, Sun MY and Xu B. 2016. Cospatial Eocene and Miocene granitoids from the Jiru Cu deposit in Tibet: Petrogenesis and implications for the formation of collisional and postcollisional porphyry Cu systems in continental collision zones. Lithos, 245: 243 – 257
Yin A and Harrison TM. 2000. Geologic evolution of the Himalayan-Tibetan orogen. Annual Review of Earth and Planetary Sciences, 28(1): 211 – 280
Yuan HL. 2012. State Key Laboratory of Continental Dynamics, Northwest University. Rock and Mineral Analysis, 31(6): 1090 – 1092 (in Chinese with English abstract)
Zheng YC, Hou ZQ, Li W, Liang W, Huang KX, Li QY, Sun QZ, Fu Q and Zhang S. 2012a. Petrogenesis and geological implications of the Oligocene Chongmuda-Mingze adakite-like intrusions and their mafic enclaves, southern Tibet. The Journal of Geology, 120(6): 647 – 669
Zheng YC, Hou ZQ, Li QY, Sun QZ, Liang W, Fu Q, Li W and Huang KX. 2012b. Origin of Late Oligocene adakitic intrusives in the southeastern Lhasa terrane: Evidence from in situ zircon U-Pb dating, Hf-O isotopes, and whole-rock geochemistry. Lithos, 148: 296 – 311
Zheng YC, Hou ZQ, Gong YL, Liang W, Sun QZ, Zhang S, Fu Q, Huang KX, Li QY and Li W. 2014. Petrogenesis of Cretaceous adakite-like intrusions of the Gangdese plutonic belt, southern Tibet: Implications for mid-ocean ridge subduction and crustal growth. Lithos, 190 – 191: 240 – 263
Zheng YY, Gao SB, Cheng LJ, Li GL, Feng NP, Fan ZH, Zhang HP, Guo JC and Zhang GY. 2004a. Finding and significances of Chongjiang porphyry copper (molybdenum, aurum) deposit, Tibet. Earth Science, 29(3): 333 – 339 (in Chinese with English abstract)
Zheng YY, Xue YX, Cheng LJ, Fan ZH and Gao SB. 2004b. Finding, characteristics and significances of Qulong superlarge porphyry copper (molybdenum) deposit, Tibet. Earth Science, 29(1): 103 – 108 (in Chinese with English abstract)
Zheng YY, Zhang GY, Xu RK, Gao SB, Pang YC, Cao L, Du AD and Shi YR. 2007. Geochronologic constraints on magmatic intrusions and mineralization of the Zhunuo porphyry copper deposit in Gangdese, Tibet. Chinese Science Bulletin, 52(22): 3139 – 3147
Zhu DC, Zhao ZD, Niu YL, Mo XX, Chung SL, Hou ZQ, Wang LQ and Wu FY. 2011. The Lhasa Terrane: Record of a microcontinent and its histories of drift and growth. Earth and Planetary Science Letters, 301(1 – 2): 241 – 255

附中文参考文献

侯增谦, 曲晓明, 黄卫, 高永丰. 2001. 冈底斯斑岩铜矿成矿带有望成为西藏第二条“玉龙”铜矿带. 中国地质, 28(10): 27 – 29, 40
侯增谦, 曲晓明, 王淑贤, 高永丰, 杜安道, 黄卫. 2003. 西藏高原冈底斯斑岩铜矿带辉钼矿 Re-Os 年龄: 成矿作用时限与动力学背景应用. 中国科学(D 辑), 33(7): 609 – 618
侯增谦, 高永丰, 孟祥金, 曲晓明, 黄卫. 2004. 西藏冈底斯中新世斑岩铜矿带: 埃达克质斑岩成因与构造控制. 岩石学报, 20(2): 239 – 248
侯增谦, 曲晓明, 杨竹森, 孟祥金, 李振清, 杨志明, 郑绵平, 郑有业, 聂凤军, 高永丰, 江思宏, 李光明. 2006a. 青藏高原碰撞造山带: Ⅲ. 后碰撞伸展成矿作用. 矿床地质, 25(6): 629 – 651
侯增谦, 赵志丹, 高永丰, 杨志明, 江万. 2006b. 印度大陆板片前缘撕裂与分段俯冲: 来自冈底斯新生代火山-岩浆作用证据. 岩石学报, 22(4): 761 – 774
侯增谦, 郑远川, 杨志明, 杨竹森. 2012. 大陆碰撞成矿作用: Ⅰ. 冈底斯新生代斑岩成矿系统. 矿床地质, 31(4): 647 – 670
黄勇, 丁俊, 李光明, 戴婕, 闫国强, 王刚, 刘晓峰. 2015. 西藏朱诺斑岩铜-钼-金矿区侵入岩锆石 U-Pb 年龄、Hf 同位素组成及其成矿意义. 地质学报, 89(1): 99 – 108
秦克章, 夏代祥, 李光明, 肖波, 多吉, 蒋光武, 赵俊兴. 2014. 西藏驱龙斑岩-夕卡岩铜钼矿床. 北京: 科学出版社, 1 – 316
芮宗瑶, 李光明, 张立生, 王龙生. 2004. 西藏斑岩铜矿对重大地质事件的响应. 地学前缘, 11(1): 145 – 152
袁洪林. 2012. 西北大学大陆动力学国家重点实验室. 岩矿测试, 31(6): 1090 – 1092
郑有业, 高顺宝, 程力军, 李国梁, 冯南平, 樊子珲, 张华平, 郭建慈, 张刚阳. 2004a. 西藏冲江大型斑岩铜钼金)矿床的发现及意义. 地球科学, 29(3): 333 – 339
郑有业, 薛迎喜, 程力军, 樊子珲, 高顺宝. 2004b. 西藏驱龙超大型斑岩铜(钼)矿床: 发现, 特征及意义. 地球科学, 29(1): 103 – 108
郑有业, 张刚阳, 许荣科, 高顺宝, 庞迎春, 曹亮, 杜安道, 石玉若. 2007. 西藏冈底斯朱诺斑岩铜矿床成岩成矿时代约束. 科学通报, 52(21): 2542 – 2548